

Iskandarovite, $\text{Sb}_6\text{O}_7(\text{SO}_4)_2$, a new antimony oxysulfate mineral from sublimates of an underground coal fire at the Fan-Yagnob coal deposit, Tajikistan

M.A. Mirakov¹, L.A. Pautov², O.I. Siidra^{3,4*}, V.Yu. Karpenko², P.Yu. Plechov², A.S. Borisov⁵

¹Umarov Physical-Technical Institute of the National Academy of Sciences of Tajikistan, Aini 299/1, 734063, Dushanbe, Tajikistan.

²Fersman Mineralogical Museum, Russian Academy of Sciences, Leninskiy pr. 18-2, 119071 Moscow, Russia.

³Department of Crystallography, St. Petersburg State University, University Emb., 7/9, St. Petersburg, 119034, Russia.

⁴Kola Science Center, Russian Academy of Sciences, Apatity, Murmansk Region, 184200 Russia, 683006, Russia.

⁵Institut für Geowissenschaften der Universität Kiel, Olshausenstr. 40, D-24098 Kiel, Germany.

* E-mail: o.siidra@spbu.ru

Abstract

A new mineral iskandarovite, $\text{Sb}_6\text{O}_7(\text{SO}_4)_2$ was discovered at the tract of Kukhi-Malik, Fan-Yagnob coal deposit, ca. 75 km N of Dushanbe, Tajikistan. Iskandarovite is an exhalative mineral formed directly from a gas of the natural underground coal fire. The mineral forms colorless prismatic crystals (50-120 μm). Mohs hardness is ~ 2.0 . Refractive indices: $\alpha = 1.985(3)$, $\beta = 2.052(5)$, $\gamma(\text{calc.}) = 2.069(9)$ (590 nm). The mineral is non-soluble in H_2O and ethanol at room temperature. Raman spectra show the absence of water, hydroxyl, carbonate, or other anions. The chemical composition determined by electron-microprobe analysis is (wt. %): $\text{Sb}_2\text{O}_3 - 82.57$; $\text{Bi}_2\text{O}_3 - 1.28$; $\text{As}_2\text{O}_3 - 0.05$; $\text{SO}_3 - 15.17$; total - 99.07. The empirical formula (based on 15 O *apfu*) is: $\text{Sb}_{5.95}\text{Bi}_{0.06}\text{As}_{0.01}\text{S}_{1.99}\text{O}_{15}$. The strongest lines of the X-ray powder diffraction pattern are (*d-I-hkl*): 10.1-40-110; 5.08-50-220; 3.26-25-311; 3.146-100-241; 2.933-73-331. Iskandarovite is orthorhombic, *Ccc2*, unit-cell parameters $a = 12.0402(3)$, $b =$

18.9599(5), $c = 5.8638(2)$ Å, $V = 1338.59(7)$ Å³, $Z = 4$, and the crystal structure was refined to $R_1 = 0.0236$ on the basis of 2053 unique reflections with $F_o > 4\sigma F_o$. The crystal structure of iskandarovite is based on sulfate tetrahedra and $[\text{O}_7\text{Sb}_6]^{4+}$ rod-like chains that are elongated along the c axis. Synthetic $\text{Sb}_6\text{O}_7(\text{SO}_4)_2$ analogue is known.

The crystal chemistry of 13 known Sb(III) sulfates and oxysulfates is reviewed.

Keywords: iskandarovite; anhydrous sulfates; antimony sulfates; oxocentered complexes; exhalative minerals; coal fires; fumaroles; Kukhi-Malik; Ravat

Introduction

A new antimony oxysulfate, $\text{Sb}_6\text{O}_7(\text{SO}_4)_2$, was found in sublimates of a natural coal fire at the tract of Kukhi-Malik, Fan-Yagnob coal deposit, central Tajikistan. The new mineral is named iskandarovite after Farukh Sheikovich Iskandarov (b. 1947). F.S. Iskandarov is a mineralogist and geologist, who has significantly contributed to the mineralogy of Tajikistan. He is an author of more than 70 research papers. F.S. Iskandarov gives lectures in mineralogy, crystallography, and thermobarogeochemistry at the Geological faculty of the Tajik State University.

The mineral is approved by the Commission on New Minerals, Nomenclature and Classification of the International Mineralogical Association (IMA 2022-034). Type material is deposited in the collections of the Fersman Mineralogical Museum, Russian Academy of Sciences, Leninskiy Prospekt 18-2, Moscow 119071, Russia, catalogue number 5845/1.

Herein, we present a description of the new mineral species and a review of the crystal chemistry of Sb sulfate minerals and synthetic compounds.

Occurrence and mineral association

Iskandarovite was collected by the authors in 2016 in sublimates of a high-temperature fumarole (gas vent) of the natural underground coal fire at the tract of Kukhi-Malik (39°18'39" N, 68°58'64" E) near the abandoned village of Ravat in the area of the Fan-Yagnob coking coal

deposit (Fig. 1). The latter is located within the Zeravshan-Gissar mountain ridge in the valley of the Yagnob river, Ayninsky district, Tajikistan, approximately 75 km north from Dushanbe. The Fan-Yagnob deposit is characterized by Triassic sedimentary rocks, Jurassic coal-bearing strata, and Cretaceous and Paleogene-Neogene deposits (Ermakov, 1935; Okhunov et al., 2017). The Fan-Yagnob deposit is one of the largest coking coal deposits in Central Asia. The Fan-Yagnob coals are characterized by their high concentrations of V, Sn, Ag, W, Cu, Mo, Pb, Zn, Cr, Be, Cd, and other elements (Novikov et al., 1989; Okhunov et al., 2017). Additionally, Ge mineralization has been described. In the vicinity of the deposit, there are numerous extinct and active underground coal fires with many active gas vents. Numerous publications (Ermakov, 1935; Vadilo, 1958; Novikov et al., 1979; 1989; Novikov, Suprychev, 1986; Belakovskiy, 1990; Sharygin et al., 2009) have investigated the geology, mineralogy, and geochemistry of the coal fires, coals, and host rocks in the Fan-Yagnob coal deposit. Extensive research on the mineralogy of the sublimates of the Kukhi-Malik coal fire resulted in the identification and detailed description of numerous rare minerals: pauflerite, bonaccite, alacranite, timmanite, cinnabar, native selenium, native tellurium, grinokite, Ge-bearing cassiterite, Se-bearing galena and cadmoindite (Mirakov et al., 2017, 2019, 2020; Pautov et al., 2019, 2022; Karpenko et al., 2021). Several new minerals, mainly sulfates, were discovered, including falgarite $K_4(VO)_3(SO_4)_5$ (Pautov et al., 2020), ermakovite $(NH_4)(As_2O_3)_2Br$ (Karpenko et al., 2023), hasanovite $KNa(MoO_2)(SO_4)_2$ (Mirakov et al., 2023), novikovite $(NH_4)_4(Mo^{+6}_2Mo^{+5}_2)_4O_8(SO_4)_5$ (Pautov et al., 2023) and sarvodaite $Al_2(SO_4)_3 \cdot 5H_2O$ (Makhmadsharif et al., 2025).

Iskandarovite forms colorless prismatic crystals (50-120 μm) (Fig. 2) on the surface of burnt siltstone. Iskandarovite is closely associated with various poorly identified Fe, Sn, Sb, and Cd sulfates, along with cadmoindite. To prevent any contact with the atmosphere, all recovered samples were immediately packed and isolated upon collection.

Physical properties

Iskandarovite has a white streak and adamantine lustre. Cleavage is perfect on {100}. Parting was not observed. Iskandarovite is transparent, with a brittle tenacity and conchoidal fracture. Iskandarovite has a Vickers Hardness Number (VHN₂₀) of 60 kg mm⁻² ($n = 5$, range 54 -65 kg mm⁻²), which approximately corresponds to a Mohs' hardness of 2.

The density of iskandarovite is > 4.26 g/cm⁻³ (Clerici liquid) and the calculated density D_{calc} is 5.166 g/cm⁻³, based on the empirical formula.

Iskandarovite is non-magnetic.

Optical Properties

The optical properties of iskandarovite were studied in West immersion liquid (West, 1936) using polarizing microscopes MIN-8 and POLAM R-213. Iskandarovite is optically biaxial (+), $\alpha = 1.985(3)$, $\beta = 2.052(5)$, $\gamma(\text{calc.}) = 2.069(9)$ (590 nm), and the measured $2V$ is $53(3)^\circ$. Pleochroism was not observed. Extinction is straight and elongation is positive $Z \parallel c$. Dispersion is weak, $r > v$. The mineral is non-pleochroic under the microscope. The Gladstone-Dale compatibility index, $1 - (K_p/K_c) = -0.008$, is superior.

Raman spectroscopy

The Raman spectrum of iskandarovite (Fig. 3) was obtained on the polished grain, which was glued to the flat glass with epoxy resin. We used a confocal Raman microscope, JY Horiba XPloRA Jobin, equipped with an Olympus BX 41 optical microscope, a diffraction grating with 1800 grooves per millimeter, and a Peltier-cooled (working temperature -51 °C), Si-based charge-coupled device (CCD) detector. Raman spectra were collected in the range 50-4000 cm⁻¹ with a 50× objective. Spatial resolution is about 5 μm. The 532 nm beam had an energy of about 25 mW. The spectra were collected at the polished surface of the unoriented crystal. No visual damage was observed on the analyzed surface of iskandarovite under these conditions after the excitation. Obtained spectra were processed using a LabSpec software, v. 5.78.24 and Fityk, v. 1.3.1.

Fourteen intensive bands were observed in the range 100-1200 cm^{-1} . The bands at 1007 cm^{-1} and 1187 cm^{-1} correspond to symmetric stretching and antisymmetric stretching vibrations, respectively, in the SO_4 anion. The band at 477 cm^{-1} corresponds to symmetric bending vibrations of the sulfate anion. Three peaks at 538, 603, and 643 cm^{-1} can be tentatively assigned as antisymmetric bending in SO_4 . The single intensive band at 930 cm^{-1} can be assigned to symmetric stretching Sb-O vibrations (Frost and Bahfenne, 2011). Bands at 331, 369, and 418 cm^{-1} correspond to O-Sb-O bending vibrations. Bands below 300 cm^{-1} are lattice vibrations. No bands were observed between 1300 and 4000 cm^{-1} which proves the absence of water, hydroxyl, carbonate, or other anions.

Chemical composition

The chemical composition of iskandarovite (6 spots) was studied by both WDS (6 spots; 20 kV, 15 nA, 5 μm beam diameter) and EDS (8 spots; 20 kV, 1 nA, 10 μm beam diameter) using JCSA-733 Jeol Superprobe at the Fersman Mineralogical Museum. Analytical results are given in Table 1. The empirical formula (based on 15 O *apfu*) is: $\text{Sb}_{5.95}\text{Bi}_{0.06}\text{S}_{1.99}\text{O}_{15}$. The ideal formula is $\text{Sb}_6\text{O}_7(\text{SO}_4)_2$, which requires Sb_2O_3 84.52, SO_3 15.48, total 100 wt.%. The mineral is insoluble in H_2O and ethanol. It dissolves slowly at room temperature in HCl 1:1.

X-ray crystallography

Powder X-ray diffraction

X-ray powder diffraction data were collected using $\text{CrK}\alpha$ – radiation, V-filter in RKU-86 camera; Ge was used as an internal standard. X-ray powder diffraction data (in \AA for $\text{CrK}\alpha$) are given in Table 2. Unit cell parameters refined from the powder data are as follows: orthorhombic, $a = 12.0591(5) \text{\AA}$, $b = 18.9618(7) \text{\AA}$, $c = 5.8681(2) \text{\AA}$, $V = 1341.82(7) \text{\AA}^3$.

Single-crystal X-ray diffraction

A single crystal of iskandarovite selected for X-ray diffraction analysis was glued onto a glass filament and arranged in a Rigaku XtaLAB Synergy-S diffractometer equipped with a

PhotonJet-S detector operating with MoK α radiation at 50 kV and 1 mA. More than a hemisphere of data was collected with a frame width of 0.5° in ω , and 80 s spent counting for each frame. The data were integrated and corrected for absorption applying a multiscan type model using the Rigaku Oxford Diffraction software CrysAlis Pro 1.171.41.104a. The unit-cell parameters were calculated by the least-squares method and the structure was solved by direct methods. The parameters of the X-ray diffraction experiment and structure refinement are given in Table 3. Atomic coordinates and displacement parameters are given in Tables 4 and 5, respectively. Selected interatomic distances are given in Table 6, and bond valences in Table 7. Lists of observed and calculated structure factors are deposited with the journal and can be downloaded from http://www.minersoc.org/pages/e_journals/dep_mat_mm.html.

Crystal structure

Cation and anion coordination

The crystal structure of iskandarovite contains three symmetrically independent Sb atoms, one S atom, and eight O sites. All Sb atoms have similar see-saw coordination of four O atoms located in one coordination hemisphere (Fig. 4). This is characteristic of the Sb³⁺ cation due to the presence of a stereochemically active 5s² lone electron pair (Gagné and Hawthorne, 2018). Sb1, Sb2, and Sb3 atoms each form four short and strong Sb-O bonds <2.40 Å (>0.34 v.u.) (bold bonds in Fig. 4). In the coordination environment of Sb2 and Sb3 atoms, oxygen atoms O6 and O7 are shared with SO₄ groups. Another coordination hemisphere of Sb atoms accommodates much weaker bonds, thereby complementing the Sb³⁺ cation environment to C.N. [11] for Sb1 and [9] for both Sb2 and Sb3. Bond-valence sums (b.v.s.) on Sb atoms fall between 2.93 and 3.03 v.u., which is close to the formal valence of Sb(III). Minor variations can be attributed to the addition of 0.16 apfu of Bi³⁺ (Table 1). The oxygen atoms O5-O8 coordinate the S⁶⁺ cation thus forming the SO₄ tetrahedron. The sulfate tetrahedron is distorted, with S–O bond lengths ranging from 1.460(6) Å (1.55 v.u.) for S1–O5 to 1.509(6) Å (1.37 v.u.) for S1–O6. These values depart significantly from the average S–O value of 1.473 Å in sulfate minerals

(Hawthorne et al., 2000). As noted above, the O6 and O7 atoms in the SO₄ tetrahedron are shared with the Sb³⁺ polyhedra.

The oxygen atoms O1, O2, O3, and O4 form bonds only with the Sb³⁺ cations. The O1 atom has a strongly distorted tetrahedral coordination thus forming {O1Sb₄}. Two short O1-Sb1 bonds (1.998(4) Å each) and two long O1-Sb1 bonds (2.759(7) Å each) are formed. The average <O–Sb> value in the {O1Sb₄} tetrahedron is 2.38 Å. Atoms O2, O3, and O4 can be considered being central in the oxocentered {OSb₃} triangles. The average values of the <O–Sb> bond lengths vary from 2.103 Å in {O3Sb₃} to 2.115 Å in {O4Sb₃}. In the triangles, the central oxygen atoms are elevated above the plane. The displacement of O atoms from the triangular plane formed by three Sb atoms (highlighted by the green dotted line in Fig. 4) is 0.34 Å for [O2Sb₃], 0.50 Å for [O3Sb₃], and 0.28 Å for [O4Sb₃].

Structure description

To facilitate comparisons between iskandarovite and related synthetic compounds and minerals, it is necessary to describe the crystal structure in terms of oxocentered tetrahedra, triangles, and SO₄ groups. Figure 5a illustrates the crystal structure of iskandarovite, which is composed of sulfate tetrahedra and [O₇Sb₆]⁴⁺ rod-like chains that are elongated along the *c* axis. {O1Sb₄} tetrahedra share one with each other via two common edges, thus forming [OSb₂]²⁺ tetrahedral chain (Fig. 5c). The latter is wrapped by the {O2Sb₃}, {O3Sb₃}, and {O4Sb₃} triangles (Fig. 5e,d). The cohesion of [O₇Sb₆]⁴⁺ rods and the SO₄ tetrahedra into a three-dimensional framework is facilitated by the Sb–O bonds with the sulfate O6 and O7 oxygen atoms. Voids filled by lone pairs are formed between the sulfate tetrahedra.

Structurally related compounds

Iskandarovite has a synthetic analogue, Sb₆O₇(SO₄)₂ (Bovin, 1976). The unit-cell volume of synthetic Sb₆O₇(SO₄)₂ is increased by 10.9 Å³ to 1349.5 Å³. The synthetic analogue exhibits a smaller distortion of the {OSb₄} tetrahedra in the single [OSb₂]⁴⁺ chain with Δ_{d_{max}–min} = 0.693 Å, whereas Δ_{d_{max}–min} = 0.761 Å for the O1–Sb bonds is observed in iskandarovite. {OSb₃} triangles

are distinguished by a larger elevation of the central O atom above the Sb_3 plane. Sulfate tetrahedra are also less distorted in the synthetic compound ($\Delta d_{\text{max-min}} = 0.035 \text{ \AA}$ for S-O bonds) compared to the mineral crystal structure ($\Delta d_{\text{max-min}} = 0.049 \text{ \AA}$ for S-O bonds). The substantial structural distortions in the mineral crystal structure are a result of the relatively high content of the large 'lone-pair' Bi^{3+} cation, as determined by microprobe analysis.

The presence of a 'lone pair' on both the Sb^{3+} and Bi^{3+} cations makes iskandarovite structurally related to several bismuth oxysalts. Iskandarovite is isostructural with the bismuth oxychromate $\text{Bi}_6\text{O}_7(\text{CrO}_4)_2$ (Grins et al., 2002). The volume of the unit-cell is enlarged from 1338 \AA^3 in iskandarovite to 1438 \AA^3 in the bismuth oxychromate. Nevertheless, the $[\text{OBi}_2]^{4+}$ single chain formed by the $\{\text{OBi}_4\}$ oxocentered tetrahedra is less distorted in the structure (Fig. 6a). The Bi-O bond lengths in the $\{\text{OBi}_4\}$ oxocentered tetrahedra range from $2.128(3) \text{ \AA}$ to $2.664(4) \text{ \AA}$ ($\Delta d_{\text{max-min}} = 0.536 \text{ \AA}$) in $\text{Bi}_6\text{O}_7(\text{CrO}_4)_2$, while the Sb-O values in iskandarovite range from $1.998(4) \text{ \AA}$ to $2.759(7) \text{ \AA}$ ($\Delta d_{\text{max-min}} = 0.761 \text{ \AA}$).

Garavelli et al. (2014) previously described rod-like $[\text{O}_7\text{Bi}_6]^{4+}$ chains in the structure of leguernite $\text{Bi}_{12.67}\text{O}_{14}(\text{SO}_4)_5 = [\text{Bi}_6\text{O}_7]_2\text{Bi}_{0.67}(\text{SO}_4)_5$, which are similar to those observed in iskandarovite. Along with $[\text{O}_7\text{Bi}_6]^{4+}$ complexes and SO_4 tetrahedra, the monoclinic structure of leguernite (Fig. 6b) also has extra Bi^{3+} sites with s.o.f. = 2/3. Furthermore, the leguernite structure contains additional sulfate groups in comparison to iskandarovite. In leguernite, each rod is surrounded by ten sulfate tetrahedra, whereas in iskandarovite, there are eight. Garavelli et al. (2014) described $[\text{Bi}_6\text{O}_7]^{4+}$ chains in leguernite as columns of $\{\text{OBi}_4\}$ tetrahedra derived from the fluorite structure. $\{\text{OBi}_3\}$ triangles that wrap the oxocentered chain were not taken into consideration.

Sb(III) sulfates - a review

The Sb(III) sulfate family has been expanded by the discovery of iskandarovite, a new natural member. There are no thorough investigations into the crystal chemistry of antimony sulfates to date. In the following concise review, we focused on Sb(III) sulfates and oxysulfates

and also those containing alkali metal cations (Table 8). It excludes compounds containing $\text{SbF}_2/\text{SbF}_3$ fluoride complexes, tetrahedral oxoanions other than sulfate, and other metal cations. The list of all compounds that were examined is given in Table 8. Furthermore, a plethora of Sb(III) sulfates have been identified (e.g., [Gospodinov and Ojkova, 1981](#); [Bergmann and Koparal, 2007](#)); however, their structures have yet to be determined.

SbO_n and OSb_m coordination polyhedra in Sb(III) sulfates and oxysulfates.

According to [Mills et al. \(2009\)](#), the coordination environment of Sb atoms may include up to 11 ligands, taking into account a cut-off distance of 3.50 Å. The stereochemical activity of the Sb $5s^2$ lone pair controls the asymmetric SbO_nE coordination of Sb(III) cations ([Walsh et al., 2011](#)). A bimodal distribution of bond-lengths in the SbO_n polyhedra is observed in Sb sulfates ([Fig. 7a](#)). The maxima are located at approximately 2.0 Å and 3.1 Å, respectively. As per [Alcock \(1972\)](#), this enables us to differentiate between primary bonds (short and strong) in one hemisphere and secondary Sb–O bonds (long and weak) in the other. Based on the statistical distribution ([Fig. 7a](#)), we selected a distance of 2.40 Å (0.34 *v.u.* using parameters from [Gagné and Hawthorne, 2015](#)) to distinguish between primary and secondary bonds. There are three primary types of $\{\text{SbO}_n\}$ polyhedra in the Sb(III) sulfates in terms of primary bonds ([Fig. 7b](#)). In several cases, the polyhedron can be classified as a transition type between $\{\text{SbO}_3\}$ and $\{\text{SbO}_4\}$, as well as between $\{\text{SbO}_4\}$ and $\{\text{SbO}_5\}$ ([Fig. 8b](#)).

Seven of the twelve Sb(III) sulfates under consideration contain 'additional' oxygen atoms ([Krivovichev et al., 2013](#)) and/or hydroxyl groups that are not part of the SO_4 polyhedra. The structures of these compounds can be described in terms of the oxocentered OSb_n polyhedra with $n = 2-4$. As shown in [Figure 7c](#), the majority of the bond lengths in oxocentered units fall between 1.9 and 2.1 Å. The most common complexes are $\{\text{OSb}_2\}$ and distorted $\{\text{OSb}_3\}$, which are supplemented by a few examples of $\{\text{OSb}_4\}$ tetrahedra ([Fig. 7d](#)). The only two structure types in which $\{\text{OSb}_4\}$ tetrahedra can be distinguished within 3.0 Å are coquandite

$\text{Sb}_{6.3}\text{O}_{8.3}(\text{SO}_4)(\text{OH})_{0.3}(\text{H}_2\text{O})_{0.7}$ (Bindi et al., 2014) and iskandarovite $\text{Sb}_6\text{O}_7(\text{SO}_4)_2$. The $\{\text{OSb}_4\}$ tetrahedra demonstrate strongly distorted geometries.

In the Sb sulfate structures, oxocentered $\{\text{OSb}_n\}$ units can be isolated or polymerized into complexes of different dimensionality. $\{\text{OSb}_2\}$ units in $\text{Sb}_2\text{O}(\text{SO}_4)_2$ are isolated. Clusters in $\text{Sb}(\text{SO}_4)(\text{OH})(\text{H}_2\text{O})$ can be described as (OH)-centered $[(\text{OH})_2\text{Sb}_2(\text{H}_2\text{O})_2]^{2+}$ units with additional H_2O molecules (Fig. 8e). Isolated complexes of edge-sharing $\{\text{OSb}_2\}$ and $\{\text{OSb}_3\}$ groups are observed in $(\text{H}_3\text{O})_2\text{Sb}_4\text{O}_3(\text{SO}_4)_4(\text{H}_2\text{O})$ (Fig. 8f) and $\text{NaSb}_3\text{O}_2(\text{SO}_4)_3(\text{H}_2\text{O})$ (Fig. 8g). The synthetic $\text{Sb}_6\text{O}_7(\text{SO}_4)_2$ (Bovin, 1976) and iskandarovite described herein contain rod-like chains of distorted tetrahedral groups wrapped by $\{\text{OSb}_3\}$ triangles. Oxocentered units form layers of various configurations in $\text{Sb}_4\text{O}_5(\text{SO}_4)$ (Fig. 8h) and klebelsbergite $\text{Sb}_4\text{O}_4(\text{SO}_4)(\text{OH})_2$ (Fig. 8i). Note that in the $\text{Sb}_4\text{O}_5(\text{SO}_4)$ structure the layers consist of both $\{\text{OSb}_2\}$ and $\{\text{OSb}_3\}$, whereas in klebelsbergite the complex layers are formed by $\{\text{OSb}_3\}$ triangles and $\{(\text{OH})\text{Sb}_2\}$ dimers. A complex three-dimensional framework consisting of all three types of units, $\{\text{OSb}_2\}$, $\{\text{OSb}_3\}$ and $\{\text{OSb}_4\}$, is observed exclusively in coquandite $\text{Sb}_{6.3}\text{O}_{8.3}(\text{SO}_4)(\text{OH})_{0.3}(\text{H}_2\text{O})_{0.7}$. The association of distorted tetrahedra via common edges into $[\text{O}_3\text{Sb}_{10}]^{24+}$ trimeric units and via common edges into $[\text{OSb}_3]^{7+}$ complexes is the unique feature of the coquandite structure (Fig. 8i,k).

Classification

The suggested classification of Sb(III) sulfates is based on the dimension of Sb–O complexes correlated with the Sb:SO₄ ratio in the structure. The cation-centered SbO_n polyhedra describe only compounds with ratios of 1:2 and 1:1. Structures with the higher content of Sb are described in terms of $[\text{O}_x\text{Sb}_y]^{z+}$ oxocentered complexes. In addition to the formation of oxocentered complexes, the structural architectures of Sb sulfates are controlled by the following factors: (1) the distinctive connectivity patterns of oxygen-antimony complexes with sulfate SO_4 groups; (2) the formation of micelles (Mackovicky, 2006) with 'lone pairs', which control the packing of sulfate tetrahedra. We assess the arrangement of micelles by examining the distribution of primary and secondary Sb–O bonds in the coordination sphere of the Sb^{3+} cation.

Sb(III) sulfates with island complexes SbO_n and OSb_n .

I. Sb:SO₄ ratio 1:2.

Three compounds, $A^+Sb(SO_4)_2$ ($A = K, Cs, H_3O$), are included in this group. These sulfates have distinct symmetries: monoclinic $KSb(SO_4)_2$ ($P2_1/c$) (Zhao et al., 2015), orthorhombic $CsSb(SO_4)_2$ ($P2_12_12_1$) (Zhao et al., 2015), and orthorhombic $(H_3O)Sb(SO_4)_2$ ($Pbc2_1$) (Mercier et al., 1983). Each of the former two phases contain a single symmetry-independent antimony atom, which forms $\{SbO_4\}$, whereas the latter contains two, $\{SbO_4\}$ and $\{SbO_5\}$. In the structure of $CsSb(SO_4)_2$ (Fig. 8a), the SbO_4 polyhedron is interconnected with SO_4 tetrahedra thus forming $[Sb(SO_4)_2]^-$ chains elongated along the a axis. Figure 8b illustrates highly corrugated $[Sb(SO_4)_2]^-$ layers with A^+ cations in the interlayer space as a result of the interconnection of $\{SbO_n\}$ polyhedra via SO_4 groups in $KSb(SO_4)_2$. A similar pattern of the structural organization is observed in $(H_3O)Sb(SO_4)_2$. $KSb(SO_4)_2$ and $(H_3O)Sb(SO_4)_2$ have different corrugation periods, which are 7.158 Å and 13.760 Å, respectively. Although the antimony sulfate complexes in the structures of $A^+Sb(SO_4)_2$ are of varying dimensionality (1D for $A = Cs^+$ and 2D for $A = K^+, H_3O^+$), the sulfate groups in the compounds have identical connectivity patterns. This connectivity includes two positions of the SO_4 tetrahedra, where each of them shares two vertices with the $\{SbO_4\}$ and/or $\{SbO_5\}$ polyhedra. Micelles in the layered $A^+Sb(SO_4)_2$ ($A = K^+, H_3O^+$) are found inside the layer (Fig. 8b), whereas those in the $CsSb(SO_4)_2$ structure (Fig. 8a) are oriented toward the large cesium cations.

II. Sb:SO₄ ratio 1:1.5.

In the $Sb_2(SO_4)_3$ structure (Fig. 8c) (Mercier et al., 1976), sulfate groups connect two symmetrically independent $\{SbO_4\}$ polyhedra via all common oxygens, thus forming a distorted mikasaite-type framework. The octahedrally coordinated Fe^{3+} cation is replaced by the 'lone pair' Sb^{3+} cation, resulting in the formation of micelles and the distortion of the mikasaite archetype. Unlike mikasaite, where all the vertices of the sulfate groups are shared with FeO_6 octahedra, sulfate tetrahedra have one or two free vertices in the framework of $Sb_2(SO_4)_3$.

III. *Sb:SO₄ ratio 1:1.*

In order to keep the formula electroneutral, the structure requires additional anions when the ratio of Sb to SO₄ is 1:1. This can be achieved by the addition of oxygen atoms and/or hydroxyl groups. Every sulfate tetrahedron in the hydrated sulfate Sb(SO₄)(OH)(H₂O) (Douglade et al., 1978) forms 0D complexes by sharing a common oxygen vertex with [(OH)₂Sb₂(H₂O)₂]⁴⁺ clusters (Fig. 8d). Micelles are located between adjacent [(OH)₂Sb₂(H₂O)₂]⁴⁺ clusters. The simplest anhydrous oxysulfate with 1:1 ratio is Sb₂O(SO₄)₂ (Mercier et al., 1975) (Fig. 8e), where isolated {OSb₂} dimers form isles via common SO₄ groups. The mineral baličžuničite Bi₂O(SO₄)₂ (Pinto et al., 2015) and its monoclinic polymorph (Aurivillius, 1988) also exhibit 1:1 ratio. However, the oxocentered bismuth complexes in both have a distinct architecture. Complexes of four {OSb₃} triangles (Fig. 7g) create a three-dimensional structure via sulfate tetrahedra in the structure of NaSb₃O₂(SO₄)₃(H₂O) (Wang et al., 2022) (Fig. 8f). In the same way, in the structure of (H₃O)₂Sb₄O₃(SO₄)₄(H₂O) (Douglade and Mercier, 1980) (Fig. 8g), complexes of two {OSb₃} triangles and one {OSb₂} dimer each (Fig. 8f) are linked via sulfate groups to form a framework. The framework channels accommodate Na⁺ or H₃O⁺ cations.

IV. *Sb:SO₄ ratio 1:0.33.*

Iskandarovite and its synthetic analog (Bovin, 1976), which are described in detail above, are characterized by the formation of one-dimensional [O₇Sb₆]⁴⁺ complexes (Fig. 9h). Micelles are formed in the framework channels, where they force the sulfate groups apart.

V. *Sb:SO₄ ratio 1:0.25.*

Continued reduction of the sulfate content is accompanied by the formation of [O₅Sb₄]²⁺ (Fig. 8g) layers in synthetic Sb₄O₅(SO₄) (Wei et al., 2021) (Fig. 9i) and [O₄OHSb₄]³⁺ (Fig. 8h) layers in klebelsbergite Sb₄O₄(SO₄)(OH)₂ (Fig. 9j) (Roper et al., 2015). In the case of Sb₄O₅(SO₄), SO₄ groups interconnect oxocentered layers into the framework. Nevertheless, the formation of micelles in klebelsbergite obstructs the formation of the framework, resulting in a predominantly layered structure.

VI. *Sb:SO₄ ratio 1:0.15.*

Coquandite $\text{Sb}_{6.3}\text{O}_{8.3}(\text{SO}_4)(\text{OH})_{0.3}(\text{H}_2\text{O})_{0.7}$ (Bindi et al., 2014) (Fig. 9k) is the sole Sb(III) oxosulfate with a 3D framework of oxocentered polyhedra. The oxocentered framework is exceedingly intricate and is formed by 41 atomic sites of ‘additional’ oxygen atoms (O21-O62, with the exception of O44, which is associated with the split Sb32 position). $[\text{O}_3\text{Sb}_{10}]^{24+}$ and $[\text{OSb}_3]^{7+}$ complexes and individual isolated $\{\text{OSb}_4\}$ tetrahedra are surrounded by $\{\text{OSb}_3\}$ triangles and $\{\text{OSb}_2\}$ dimers via common Sb atoms, forming large blocks parallel to the *ab* plane (Fig. 9k). $\{\text{OSb}_4\}$ tetrahedra and $\{\text{OSb}_3\}$ triangles interconnect the blocks into an antimony-oxide framework with water and hydroxyl associating in the channels. In coquandite, sulfate tetrahedra have little effect on the three-dimensional integrity of the structure. The coquandite structure can be described as the incorporation of sulfate groups into the Sb_2O_3 matrix, which is followed by a sequence of distortions and transformations.

Conclusions

Iskandarovite is the third mineral identified to date in the family of antimony sulfates. Its crystallization from gas is unusual. Klebelsbergite and coquandite are two other minerals that are hydrated and are formed as the result of the alteration of stibnite. $\text{Sb}_2(\text{SO}_4)_3$, though not yet described as a mineral, is also known as a product of stibnite oxidation at approximately 116 °C (Štrbac et al., 2010). Bovin (1976) reported the synthesis of a synthetic analogue of iskandarovite from a 6 M sulfuric acid solution. Similarly, $(\text{H}_3\text{O})\text{Sb}(\text{SO}_4)_2$ crystals were also formed from highly acidic H_2SO_4 solutions (Mercier et al., 1983). $(\text{H}_3\text{O})\text{Sb}(\text{SO}_4)_2$ crystals are unstable in air and promptly transform into the anhydrous $\text{Sb}_2\text{O}(\text{SO}_4)_2$. In contrast, $A^+\text{Sb}(\text{SO}_4)_2$ crystals containing K^+ and Cs^+ cations are stable in air (Zhao et al., 2015). The discovery and description of iskandarovite in coal fires showcase the potential of gas-transport methods for the formation of anhydrous non-centrosymmetric antimony sulfates and subsequent studies.

The antimony sulfates structural classification shows a variety of structure types. 7 out of 12 compounds are non-centrosymmetric, which indicates that the synthesis of compounds in this

family has promising prospects for the discovery of nonlinear optical materials. That is to be expected for the Sb^{3+} cation that has a $5s^2$ 'lone pair'. Both cation- and anion-centered Sb–O complexes have dimensionalities that range from $0D$ at 1:2 in $\text{KSb}(\text{SO}_4)_2$ to $3D$ at 1:0.15 in coquandite, which correlates with the Sb:(SO_4) ratio. In the most of the structures that have been examined, the Sb–O complexes are isolated ($0D$). When the Sb:(SO_4) ratio is 1:1 or higher, all structures contain 'additional' (non-sulfate) oxygen atoms, resulting in the formation of oxocentered complexes $[\text{O}_x\text{Sb}_y]^{z+}$. Description in terms of oxocentered units allows us to reveal structural relationships with other oxysalts of 'lone pair' cations (e.g. Bi^{3+}). Table 8 demonstrates that the dimensionality of Sb–O complexes is increased from one order ($0D \rightarrow 1D$, $2D \rightarrow 3D$) to three orders ($0D \rightarrow 3D$) as a result of the cohesion by SO_4 tetrahedra. Consequently, SO_4 groups act as condensing building blocks in antimony sulfate crystal structures, in both natural minerals and synthetic compounds.

Acknowledgements

We thank S. Yorov, S. Mahmasharif and M.A. Shodibekov for their help in organization of fieldwork. This work was financially supported by the Russian Science Foundation through the grant 25-17-00157 (for OIS). Technical support by the SPbSU X-ray Diffraction Resource Center (project # 118201839) is gratefully acknowledged.

References

1. Alcock N.W. (1972) Secondary bonding to nonmetallic elements. *Advances in Inorganic Chemistry and Radiochemistry*, **15**, 1–57.
2. Aurivillius, B. (1988) Pyrolysis products of $\text{Bi}_2(\text{SO}_4)_3$. II. Crystal structure of $\text{Bi}_2\text{O}(\text{SO}_4)_2$. *Acta Chemica Scandinavica A*, **42**, 95–110.
3. Belakovski D. Die Mineralien der brennenden Kohleflöze von Ravat in Tadshikistan. *Lapis*, 1990, **15**, 21–26.

4. Bergmann M.E.H. and Koparal A.S. (2007) Kinetic studies on electrochemical antimony removal from concentrated sulfuric acid systems. *Chemical Engineering and Technology*, **30**, 242–249.
5. Bindi L., Biagioni C., Ceccantini L., Batoni M., Menchetti S. (2014) Coquandite, $\text{Sb}_{6+x}\text{O}_{8+x}(\text{SO}_4)(\text{OH})_x \cdot (\text{H}_2\text{O})_{1-x}$ ($x = 0.3$), from the Cetine mine, Tuscany, Italy: crystal structure and revision of the chemical formula. *Mineralogical Magazine*, **78**, 871–888.
6. Bovin J.-O. (1976) The crystal structure of the antimony(III) oxide sulphate $\text{Sb}_6\text{O}_7(\text{SO}_4)_2$. *Acta Crystallographica*, **B32**, 1771–1777.
7. Douglade J. and Mercier R. (1980) Structure du tétrasulfate d'hydroxodioxotétraantimoine(III) et de dioxonium monohydraté $\text{Sb}^{\text{III}}_4\text{O}_2(\text{OH})(\text{SO}_4)_4(\text{H}_5\text{O}_2) \cdot \text{H}_2\text{O}$ (ou $\text{Sb}_2\text{O}_3 \cdot 2\text{SO}_3 \cdot 2\text{H}_2\text{O}$). *Acta Crystallographica*, **B36**, 2919–2925 [in French].
8. Douglade J., Mercier R. and Vivier H. (1978) Structure cristalline de $\text{Sb}_2(\text{OH})_2(\text{SO}_4)_2 \cdot 2\text{H}_2\text{O}$ (ou $\text{Sb}_2\text{O}_3 \cdot 2\text{SO}_3 \cdot 3\text{H}_2\text{O}$). *Acta Crystallographica*, **B34**, 3163–3168 [in French].
9. Ermakov N.P. (1935) Pasrud-Yagnobskoye coal deposit and coal-seam fires of the Kantag mountain. Pp. 47–66 in: On geology of coal deposits of Tajikistan. *Materials of Tadjik-Pamir Expedition*, Vol. **12** [in Russian].
10. Frost R.L. and Bahfenne S. (2011). A Raman spectroscopic study of the antimony mineral klebelsbergite $\text{Sb}_4\text{O}_4(\text{OH})_2(\text{SO}_4)$. *Journal of Raman Spectroscopy*, **42**, 219–223.
11. Gagné O.C. and Hawthorne F.C. (2015) Comprehensive derivation of bond-valence parameters for ion pairs involving oxygen. *Acta Crystallographica*, **B71**, 562–578.
12. Gagné O.C. and Hawthorne F.C. (2018) Bond-length distributions for ions bonded to oxygen: results for the non-metals and discussion of lone-pair stereoactivity and the polymerization of PO_4 . *Acta Crystallographica*, **B74**, 79–96.

13. Garavelli A., Pinto D., Mitolo D. and Bindi L. (2014) Leguernite, $\text{Bi}_{12.67}\text{O}_{14}(\text{SO}_4)_5$, a new Bi oxysulfate from the fumarole deposit of La Fossa crater, Vulcano, Aeolian Islands, Italy. *Mineralogical Magazine*, **78**, 1629–1645.
14. Gospodinov G. and Ojkova D.T. (1981) Untersuchung der Phasengleichgewichte in den Systemen $\text{Sb}_2\text{O}_3\text{--SO}_3\text{--H}_2\text{O}$ und $\text{Bi}_2\text{O}_3\text{--SO}_3\text{--H}_2\text{O}$. *Zeitschrift für anorganische und allgemeine Chemie*, **472**, 233–240 [in German].
15. Grins J., Esmaeilzadeh S. and Hull S. (2002) Structure and ionic conductivity of $\text{Bi}_6\text{Cr}_2\text{O}_{15}$, a new structure type containing $(\text{Bi}_{12}\text{O}_{14})^{8n+}_n$ columns and CrO_4^{2-} tetrahedra. *Journal of Solid State Chemistry*, **163**, 144–150.
16. Hawthorne F.C., Krivovichev S.V. and Burns P.C. (2000) The crystal chemistry of sulfate minerals. *Reviews in Mineralogy and Geochemistry*, **40**, 1–112.
17. Karpenko V.Y., Pautov L.A., Siidra O.I., Mirakov M.A., Zaitsev A.N., Plechov P.Y. and Makhmadsharif S. (2023) Ermakovite $(\text{NH}_4)(\text{As}_2\text{O}_3)_2\text{Br}$, a new exhalative arsenite bromide mineral from the Fan-Yagnob coal deposit, Tajikistan. *Mineralogical Magazine*, **87**, 69–78.
18. Karpenko V.Yu., Pautov L.A., Mirakov M.A., Siidra O.I., Makhmadsharif S., Shodibekov M. and Plechov P.Yu. (2021) Bonazziite and alacranite from sublimates of the natural underground coal fire at Kukhi-Malik tract, Tajikistan. *New Data on Minerals*, **54**, 82–93 [in Russian].
19. Krivovichev S.V., Mentré O., Siidra O.I., Colmont M. and Filatov S.K. (2013) Anion-centered tetrahedra in inorganic compounds. *Chemical Reviews*, **113**, 6459–6535.
20. Makhmadsharif S., Pautov L.A., Siidra O.I., Mirakov M.A., Karpenko V.Y. and Shodibekov M.A. (2024) Sarvodaite $\text{Al}_2(\text{SO}_4)_3 \cdot 5\text{H}_2\text{O}$, a new mineral from the Fan-Yagnob coal deposit, Tajikistan. *Mineralogical Magazine*, doi:10.1180/mgm.2025.10165.

21. Makovicky E. (2006) Crystal structures of sulfides and other chalcogenides. *Reviews in Mineralogy and Geochemistry*, **61**, 7–125.
22. Mercier R., Douglade J. and Bernard J. (1976) Structure cristalline de $\text{Sb}_2\text{O}_3 \cdot 3\text{SO}_3$. *Acta Crystallographica*, **B32**, 2787–2791 [in French].
23. Mercier R., Douglade J. and Theobald F. (1975) Structure cristalline de $\text{Sb}_2\text{O}_3 \cdot 2\text{SO}_3$. *Acta Crystallographica*, **B31**, 2081–2085 [in French].
24. Mercier R., Douglade J., Jones P.G. and Sheldrick G.M. (1983) Structure of an oxonium antimony(III) sulphate, $(\text{H}_3\text{O})_2\text{Sb}_2(\text{SO}_4)_4$. *Acta Crystallographica*, **C39**, 145–148.
25. Mills S.J., Christy A.G., Chen E.C.-C. and Raudsepp M. (2009) Revised values of the bond valence parameters for $^{[6]}\text{Sb(V)}\text{--O}$ and $^{[3-11]}\text{Sb(III)}\text{--O}$. *Zeitschrift für Kristallographie*, **224**, 423–431.
26. Mirakov M.A., Faiziev A.R. and Pautov L.A. (2017) Native selenium in products of the underground fire of the Fan-Yagnob coal field (the Central Tajikistan). *Doklady Akademii Nauk Tadzhikskoy Respubliki*, **60**, 456–460 [in Russian].
27. Mirakov M.A., Pautov L.A., Karpenko V.Yu., Faiziev A.R. and Makhmadsharif S. (2019) Pauflerite $\beta\text{-VO}(\text{SO}_4)$ from sublimations of the natural underground fire at Kukhi-Malik (Ravat) tract, Fan-Yagnob coal deposit, Tajikistan. *New Data on Minerals*, **53**, 114–120 [in Russian].
28. Mirakov M.A., Pautov L.A., Mahmadsharif S. Karpenko V.Yu. and Shodibekov M.A. (2020) The first find of mercury minerals - tiemannite and cinnabar in the sublimates of a natural underground fire in the Kuhi-Malik tract at the Fan-Yagnob coal. *New Data on Minerals*, **54**, 96–106 [in Russian].
29. Mirakov M.A., Pautov L.A., Siidra O.I., Makhmadsharif S., Karpenko V.Y., Plechov P.Y. (2023) Hasanovite $\text{KNa}(\text{MoO}_2)(\text{SO}_4)_2$, a new mineral from natural underground coal fires at the Fan-Yagnob Coal Deposit, Tajikistan. *Zapiski Vserossijskogo mineralogicheskogo obshchestva*, **152**, 18–36 [in Russian].

30. Novikov V.P. and Suprychev V.V. (1986) Conditions of the modern mineral genesis at the underground firing coals at Fan-Yagnobskoye deposit. *Mineralogiya Tadzhikistana*, **7**, 91–104 [in Russian].
31. Novikov V.P., Suprychev V.V. and Babayev M.A. (1979) Salammoniac from sublimates of the underground coal fire at the Ravat coal deposit (Central Tadzhikistan). *Doklady Akademii nauk Tadzhikskoyi SSR*, **12**, 687–960 [in Russian].
32. Novikov V.P., Suprychev V.V. and Salikhov F.S. (1989) Some geochemical specific of the supergene mineral origin in the conditions of the modern coal fire on the example of Fan-Yagnobskoye deposit. *Mineralogiya of Tadzhikistana*, **8**, 107–118 [in Russian].
33. Okhunov R.V., Yorov Z.Yo. and Negmatov I.I. (2017) Atlas reference book of the Fan-Yagnob coal deposit. Dushanbe, 170 p. [in Russian].
34. Pautov L.A., Mirakov M.A., Karpenko V.Yu. and Mahmadsarif S. (2022) Ge-bearing cassiterite from sublimates of a natural underground fire in the Kukhi-Malik tract in the Ravat area of the Fan-Yagnob coal deposit (Tajikistan). *New Data on Minerals*, **56**, 12–23 [in Russian].
35. Pautov L.A., Mirakov M.A., Mahmadsarif S., Karpenko V.Yu. and Faiziev A.R. (2019) The find of native tellurium in the sublimates of a natural underground fire at the Fan-Yagnob coal deposit (Tadzhikistan). *New Data on Minerals*, **53**, 95–99 [in Russian].
36. Pautov L.A., Mirakov M.A., Siidra O.I., Chukanov N.V., Borisov A.S., Karpenko V.Y., Plechov P.Y. and Makhmadsharif S. (2023) Novikovite, IMA 2022-067. CNMNC Newsletter 70. *Mineralogical Magazine*, **87**.
37. Pautov L.A., Mirakov M.A., Siidra O.I., Faiziev A.R., Nazarchuk E.V, Karpenko V.Y.u. and Makhmadsharif S. (2020) Falgarite, $K_4(VO)_3(SO_4)_5$, a new mineral from sublimates of a natural underground coal fire at the tract of Kukhi-Malik, Fan-Yagnob coal deposit, Tajikistan. *Mineralogical Magazine*, **84**, 455–462.

38. Pinto D., Garavelli A. and Balić-Žunić T. (2015) The crystal structure of baličžunićite, $\text{Bi}_2\text{O}(\text{SO}_4)_2$, a new natural bismuth oxide sulfate. *Mineralogical Magazine*, **79**, 597–611.
39. Roper A.J., Leverett P., Murphy T.D., Williams P.A. and Hibbs D.E. (2015) Klebelsbergite, $\text{Sb}_4\text{O}_4\text{SO}_4(\text{OH})_2$: Stability relationships, formation in Nature, and refinement of its structure. *American Mineralogist*, **100**, 602–607.
40. Sharygin V.V., Sokol E.V. and Belakovski D.I. (2009) Fayalite-sekaninaite paralava from the Ravat coal fire (central Tajikistan). *Russian Geology and Geophysics*, **50**, 703–721.
41. Štrbac N., Mihajlović I., Minić D. and Živković Ž. (2010) Characterization of the natural mineral form from the PbS – Sb_2S_3 system. *Journal of Mining and Metallurgy*, **46**, 75–86.
42. Vadilo P.S. (1958) The underground fire in Central Tajikistan. *Priroda*, **8**, 88–91 [in Russian].
43. Walsh A., Payne D.J., Egdell R.G. and Watson G.W. (2011) Stereochemistry of post-transition metal oxides: revision of the classical lone pair model. *Chemical Society Reviews*, **40**, 4455–4463.
44. Wang K., Li X.-F., He C., Li J.-H., An X.-T., Wei L., Wei Q. and Wang G.-M. (2022) $\text{NaSb}_3\text{O}_2(\text{SO}_4)_3 \cdot \text{H}_2\text{O}$: A new alkali-metal antimony(III) sulfate with a unique $\text{Sb}_6\text{O}_{20}\text{H}_4$ unit and moderate birefringence. *Crystal Growth & Design*, **22**, 478–484.
45. Wei Q., Wang K., He C., Wei L., Li X.-F., Zhang S., An X.-T., Li J.-H. and Wang G.-M. (2021) Linear and nonlinear optical properties of centrosymmetric $\text{Sb}_4\text{O}_5\text{SO}_4$ and noncentrosymmetric $\text{Sb}_4\text{O}_4(\text{SO}_4)(\text{OH})_2$ induced by lone pair stereoactivity. *Inorganic Chemistry*, **60**, 11648–11654.
46. West C.D. (1936). Immersion liquids of high refractive index. *American Mineralogist*, **21**, 245-249.
47. Zhao X., Mei D., Xu J. and Wu Y. (2015) Synthesis, crystal structures of $\text{ASb}(\text{SO}_4)_2$ ($A = \text{K}, \text{Cs}$). *Solid State Sciences*, **50**, 52–57.

Table 1. Chemical composition ($n = 6$) (wt.%) for iskandarovite.

| Constituent | wt% | Range | SD | Probe Standard |
|--------------------------------|-------|----------------|------|--------------------------------|
| Sb ₂ O ₃ | 82.57 | 79.56 - 84.58 | 0.40 | Sb ₂ O ₃ |
| Bi ₂ O ₃ | 1.28 | 0.10 - 3.47 | 0.08 | Bi ₂ O ₃ |
| SO ₃ | 15.17 | 14.66 - 15.54 | 0.14 | BaSO ₄ |
| Total | 99.02 | 97.58 - 100.22 | | |

Table 2. Powder X-ray diffraction data for iskandarovite.

| I_{meas} | d_{meas} | I_{calc} | d_{calc} | h | k | l | I_{meas} | d_{meas} | I_{calc} | d_{calc} | h | k | l |
|-------------------|-------------------|-------------------|-------------------|----------|----------|----------|-------------------|-------------------|-------------------|-------------------|----------|-----------|----------|
| 40 | 10.1 | 36 | 10.164 | 1 | 1 | 0 | 8 | 2.186 | 3 | 2.180 | 4 | 6 | 0 |
| 20 | 9.6 | 9 | 9.480 | 0 | 2 | 0 | 10 | 2.146 | 5 | 2.149 | 0 | 6 | 2 |
| 10 | 5.59 | 1 | 5.596 | 1 | 3 | 0 | 14 | 2.105 | 1 | 2.101 | 5 | 3 | 1 |
| 50 | 5.08 | 19 | 5.082 | 2 | 2 | 0 | 10 | 2.059 | 3 | 2.051 | 4 | 2 | 2 |
| 5 | 4.05 | 4 | 4.048 | 1 | 3 | 1 | 25 | 2.044 | 8 | 2.043 | 4 | 6 | 1 |
| 2 | 3.95 | 6 | 3.926 | 3 | 1 | 0 | 20 | 1.962 | 3 | 1.963 | 1 | 7 | 2 |
| 23 | 3.84 | 16 | 3.840 | 2 | 2 | 1 | 10 | 1.923 | 1 | 1.921 | 5 | 5 | 1 |
| 10 | 3.63 | 5 | 3.617 | 1 | 5 | 0 | 12 | 1.863 | 3 | 1.862 | 4 | 8 | 0 |
| 25 | 3.26 | 3 | 3.263 | 3 | 1 | 1 | 22 | 1.85 | 7 | 1.852 | 5 | 1 | 2 |
| 100 | 3.146 | 100 | 3.144 | 2 | 4 | 1 | 6 | 1.829 | 5 | 1.824 | 2 | 2 | 3 |
| 6 | 3.08 | 12 | 3.078 | 1 | 5 | 1 | 24 | 1.801 | 12 | 1.800 | 5 | 7 | 0 |
| 3 | 3.01 | 9 | 3.010 | 4 | 0 | 0 | 5 | 1.756 | 2 | 1.750 | 3 | 1 | 3 |
| 73 | 2.933 | 45 | 2.934 | 3 | 3 | 1 | 3 | 1.73 | 3 | 1.731 | 2 | 4 | 3 |
| 18 | 2.82 | 8 | 2.817 | 1 | 1 | 2 | 17 | 1.727 | 6 | 1.728 | 2 | 10 | 1 |
| 10 | 2.8 | 5 | 2.801 | 0 | 2 | 2 | 7 | 1.695 | 4 | 1.694 | 1 | 9 | 2 |
| 17 | 2.636 | 5 | 2.643 | 1 | 7 | 0 | 12 | 1.632 | 5 | 1.631 | 6 | 2 | 2 |
| 15 | 2.583 | 7 | 2.577 | 4 | 2 | 1 | 5 | 1.617 | 4 | 1.615 | 4 | 2 | 3 |
| 12 | 2.54 | 5 | 2.540 | 2 | 2 | 2 | 32 | 1.601 | 2 | 1.602 | 2 | 6 | 3 |
| 12 | 2.495 | 6 | 2.495 | 3 | 5 | 1 | 12 | 1.598 | 12 | 1.597 | 7 | 3 | 1 |
| 10 | 2.4 | 11 | 2.389 | 5 | 1 | 0 | 9 | 1.575 | 2 | 1.574 | 3 | 9 | 2 |
| 33 | 2.372 | 11 | 2.370 | 0 | 8 | 0 | 30 | 1.532 | 10 | 1.529 | 3 | 11 | 1 |
| 12 | 2.354 | 3 | 2.349 | 3 | 1 | 2 | 8 | 1.514 | 4 | 1.513 | 7 | 5 | 1 |
| 10 | 2.28 | 5 | 2.278 | 1 | 5 | 2 | 12 | 1.479 | 5 | 1.479 | 2 | 12 | 1 |
| 5 | 2.217 | 2 | 2.217 | 3 | 3 | 2 | | | | | | | |

Table 3. Crystallographic data and refinement parameters for iskandarovite.

| Crystal data | |
|---|--|
| Formula | Sb ₆ O ₇ (SO ₄) ₂ |
| Crystal system | Orthorhombic |
| Space group | <i>Ccc</i> 2 (no. 37) |
| Unit cell dimensions <i>a</i> , <i>b</i> , <i>c</i> (Å) | 12.0402(3), 18.9599(5), 5.8638(2) |
| Unit-cell volume (Å ³) | 1338.59(7) |
| <i>Z</i> | 4 |
| Absorption coefficient (mm ⁻¹) | 12.333 |
| Crystal size (mm) | 0.08×0.04×0.02 |
| Data collection | |
| Temperature (K) | 296 |
| Radiation, wavelength (Å) | MoK α , 0.71073 |
| <i>F</i> (000) | 1832 |
| θ range (°) | 3.384 – 33.704 |
| <i>h</i> , <i>k</i> , <i>l</i> ranges | –16→18, –22→28, –8→8 |
| Total reflections collected | 5843 |
| Unique reflections (<i>R</i> _{int}) | 2082 (0.017) |
| Unique reflections <i>F</i> > 4 σ (<i>F</i>) | 2053 |
| Structure refinement | |
| Refinement method | Full-matrix least-squares on <i>F</i> ² |
| Weighting coefficients <i>a</i> , <i>b</i> | 0.0429, 0.5638 |
| Data/restraints/parameters | 2082 /0/106 |
| <i>R</i> ₁ [<i>F</i> > 4 σ (<i>F</i>)], <i>wR</i> ₂ [<i>F</i> > 4 σ (<i>F</i>)] | 0.0236, 0.0585 |
| <i>R</i> ₁ all, <i>wR</i> ₂ all | 0.0239, 0.0587 |
| Gof on <i>F</i> ² | 1.050 |
| Largest diff. peak and hole (<i>e</i> Å ⁻³) | 1.073, –1.901 |

Table 4. Coordinates and isotropic displacement parameters (Å) of atoms in iskandarovite.

| <i>Atom</i> | <i>Wyck.</i> | <i>x</i> | <i>y</i> | <i>z</i> | <i>U</i> _{eq} |
|-------------|--------------|-------------|-------------|-------------|------------------------|
| Sb1 | 8 <i>d</i> | 0.89176(3) | 0.93386(2) | 0.99922(7) | 0.00868(10) |
| Sb2 | 8 <i>d</i> | 0.31260(3) | 0.93478(2) | 0.88752(9) | 0.00960(10) |
| Sb3 | 8 <i>d</i> | 0.90718(3) | 0.79289(2) | 0.36918(10) | 0.01043(10) |
| S1 | 8 <i>d</i> | 0.63341(13) | 0.84477(7) | 0.8373(3) | 0.0132(3) |
| O1 | 4 <i>a</i> | 0 | 0 | 0.1440(16) | 0.0108(10) |
| O2 | 8 <i>d</i> | 0.7582(3) | 0.9988(2) | 0.1116(10) | 0.0107(8) |
| O3 | 8 <i>d</i> | 0.1535(3) | 0.8984(2) | 0.8240(8) | 0.0091(8) |
| O4 | 8 <i>d</i> | 0.9932(4) | 0.83510(18) | 0.1040(9) | 0.0111(8) |
| O5 | 8 <i>d</i> | 0.6926(5) | 0.8330(3) | 0.0513(11) | 0.0303(14) |
| O6 | 8 <i>d</i> | 0.7155(4) | 0.8447(2) | 0.6428(10) | 0.0190(10) |
| O7 | 8 <i>d</i> | 0.5563(6) | 0.7862(3) | 0.7902(13) | 0.0410(18) |
| O8 | 8 <i>d</i> | 0.5768(4) | 0.9131(3) | 0.8361(12) | 0.0275(14) |

Table 5. Anisotropic displacement parameters (Å) of atoms in iskandarovite.

| Atom | U^{11} | U^{22} | U^{33} | U^{23} | U^{13} | U^{12} |
|------|-------------|-------------|-----------|--------------|--------------|--------------|
| Sb1 | 0.00890(16) | 0.00987(18) | 0.0073(2) | -0.00056(14) | -0.00004(16) | -0.00016(11) |
| Sb2 | 0.00708(15) | 0.01111(17) | 0.0106(2) | -0.00168(18) | -0.00075(16) | 0.00192(10) |
| Sb3 | 0.01195(16) | 0.01054(17) | 0.0088(2) | 0.00019(15) | -0.00073(17) | -0.00433(11) |
| S1 | 0.0141(6) | 0.0156(6) | 0.0098(8) | 0.0001(5) | -0.0010(6) | -0.0079(5) |
| O1 | 0.010(2) | 0.012(2) | 0.010(3) | 0 | 0 | -0.004(2) |
| O2 | 0.0102(14) | 0.0096(14) | 0.012(2) | 0.0016(14) | 0.0011(19) | 0.0033(17) |
| O3 | 0.0078(15) | 0.0113(16) | 0.008(2) | 0.0017(14) | -0.0009(15) | -0.0006(13) |
| O4 | 0.0134(17) | 0.0114(16) | 0.009(2) | -0.0005(18) | 0.0026(16) | 0.0022(17) |
| O5 | 0.038(3) | 0.039(4) | 0.014(3) | -0.001(2) | -0.010(2) | 0.000(3) |
| O6 | 0.023(2) | 0.0155(19) | 0.019(3) | 0.005(2) | 0.009(2) | -0.0003(17) |
| O7 | 0.046(4) | 0.046(4) | 0.031(4) | -0.006(3) | 0.006(3) | -0.037(3) |
| O8 | 0.023(2) | 0.029(3) | 0.030(4) | 0.001(2) | 0.005(2) | 0.006(2) |

Table 6. Selected interatomic distances (Å) in iskandarovite.

| | | | | | | | |
|-------------|----------|--------|----------|--------|----------|--------|----------|
| Sb1–O1 | 1.998(4) | Sb2–O2 | 2.010(5) | Sb3–O4 | 1.994(5) | S1–O5 | 1.460(6) |
| Sb1–O3 | 2.092(5) | Sb2–O3 | 2.070(4) | Sb3–O4 | 2.033(5) | S1–O8 | 1.465(5) |
| Sb1–O2 | 2.130(4) | Sb2–O2 | 2.195(5) | Sb3–O3 | 2.146(4) | S1–O7 | 1.473(5) |
| Sb1–O4 | 2.319(4) | Sb2–O6 | 2.296(5) | Sb3–O7 | 2.385(5) | S1–O6 | 1.509(6) |
| Sb1–O1 | 2.759(7) | Sb2–O5 | 2.760(6) | Sb3–O7 | 2.922(7) | | |
| Sb1–O2 | 3.063(5) | Sb2–O8 | 2.977(7) | Sb3–O6 | 2.978(5) | | |
| Sb1–O5 | 3.082(6) | Sb2–O8 | 3.191(6) | Sb3–O5 | 3.258(6) | | |
| Sb1–O4 | 3.285(5) | Sb2–O8 | 3.221(5) | Sb3–O5 | 3.275(6) | | |
| Sb1–O3 | 3.383(4) | Sb2–O8 | 3.521(7) | Sb3–O6 | 3.400(5) | | |
| Sb1–O3 | 3.387(4) | | | | | | |
| Sb1–O6 | 3.425(6) | | | | | | |
| O1–Sb1 (×2) | 1.998(4) | O2–Sb2 | 2.010(5) | O3–Sb2 | 2.070(4) | O4–Sb3 | 1.994(5) |
| O1–Sb1 (×2) | 2.759(7) | O2–Sb1 | 2.130(4) | O3–Sb1 | 2.092(5) | O4–Sb3 | 2.033(5) |
| | | O2–Sb2 | 2.195(5) | O3–Sb3 | 2.146(4) | O4–Sb1 | 2.319(4) |

Table 7. Bond-valence analysis (in valence units = *v.u.*) for the crystal structure of iskandarovite.

| | O1 | O2 | O3 | O4 | O5 | O6 | O7 | O8 | Σ |
|------------|--------------------|--------------|--------------|--------------|-------------|-------------|-------------|------------------------------|-------------|
| Sb1 | 0.86×2↓ 0.15×2↓ | 0.63 0.07 | 0.69 0.04 | 0.41 0.04 | 0.07 | 0.03 | | | 3.03 |
| Sb2 | | 0.84 0.55 | 0.73 | | 0.15 | 0.43 | | 0.09 0.06 0.05 0.03 | 2.93 |
| Sb3 | | | 0.61 | 0.87 | 0.05 | 0.09 | 0.35 | | 2.94 |
| S1 | | | | 0.79 | 0.05 | 0.03 | 0.10 | | 5.95 |
| Σ | 2.02 | 2.09 | 2.11 | 2.11 | 1.87 | 1.95 | 1.95 | 1.76 | |

Table 8. Crystallographic parameters of Sb(III) sulfate synthetic compounds and minerals.

| Chemical formula/ Mineral name | Sb:SO ₄ | Sb-O complex | Sulfate Structure | SG | <i>a</i> , Å <i>α</i> , ° | <i>b</i> , Å <i>β</i> , ° | <i>c</i> , Å <i>γ</i> , ° | <i>V</i> , Å ³ | Referenc e |
|---|--------------------|-----------------|----------------------|---|------------------------------|------------------------------|------------------------------|---------------------------|--|
| KSb(SO ₄) ₂ | 1:2 | 0D | 2D | <i>P</i> 2 ₁ / <i>c</i> | 10.6745(18) | 7.1579(12) 91.466(3) | 8.7597(15) | 669.1(2) | Zhao et al., 2015 |
| CsSb(SO ₄) ₂ | 1:2 | 0D | 1D | <i>P</i> 2 ₁ 2 ₁ 2 ₁ | 5.2429(8) | 9.5942(16) | 14.850(2) | 746.98(20) | Zhao et al., 2015 |
| (H ₃ O)Sb(SO ₄) ₂ | 1:2 | 0D | 2D | <i>Pbc</i> 2 ₁ | 11.085(2) | 13.760(2) | 8.919(3) | 1360.40 | Mercier et al., 1983 |
| Sb ₂ (SO ₄) ₃ | 1:1.5 | 0D | 3D | <i>P</i> 2 ₁ / <i>c</i> | 13.12(2) | 4.750(5) 126.50(25) | 17.55(3) | 881.46 | Mercier et al., 1976 |
| Sb(SO ₄)(OH)(H ₂ O) | 1:1 | 0D | 0D | <i>P</i> 2 ₁ / <i>c</i> | 6.516(1) | 13.163(1) 126.09(1) | 6.798(1) | 471.17 | Douglade et al., 1978 |
| Sb ₂ O(SO ₄) ₂ | 1:1 | 0D | 0D | <i>P</i> 4 ₁ 2 ₁ 2 | 6.59(1) | | 17.04(3) | 740.01 | Mercier et al., 1975 |
| NaSb ₃ O ₂ (SO ₄) ₃ (H ₂ O) | 1:1 | 0D | 3D | <i>P</i> -1 | 6.5853(7) 104.995(9) | 9.8327(8) 94.466(9) | 10.1884(12) 101.354(8) | 619.0(1) | Wang et al., 2022 |
| (H ₃ O) ₂ Sb ₄ O ₅ (SO ₄) ₄ (H ₂ O) | 1:1 | 0D | 3D | <i>Pna</i> 2 ₁ | 18.835(8) | 9.629(6) | 9.774(5) | 1773.00 | Douglade and Mercier, 1980 |
| Sb ₆ O ₇ (SO ₄) ₂ iskandarovite | 1:0.33 | 1D | 3D | <i>Ccc</i> 2 | 12.0402(3) | 18.9599(5) | 5.8638(2) | 1338.59(7) | This work |
| Sb ₆ O ₇ (SO ₄) ₂ (synthetic) | 1:0.33 | 1D | 3D | <i>Ccc</i> 2 | 12.073(2) | 19.023(4) | 5.876(1) | 1349.50 | Bovin, 1976 |
| Sb ₄ O ₅ (SO ₄) | 1:0.25 | 2D | 3D | <i>Pbca</i> | 14.0090(7) | 9.0717(5) | 14.1976(7) | 1804.31(16) | Wei et al., 2021 |
| Sb ₄ O ₄ (SO ₄)(OH) ₂ klebelsbergite | 1:0.25 | 2D | 2D | <i>Pca</i> 2 ₁ | 5.7563(4) | 11.2538(7) | 14.8627(9) | 962.81(11) | Roper et al., 2015 Wei et al., 2021 |
| Sb _{6+x} O _{8+x} (SO ₄)(OH) _x (H ₂ O) _{1-x} (<i>x</i> = 0.3) coquandite | 1:0.15 | 3D | 3D | <i>P</i> -1 | 11.4292(5) 91.152(3) | 29.772(1) 119.266(4) | 11.2989(5) 92.624(3) | 3346.4(2) | Bindi et al., 2014 |



Figure 1. The Kukhi-Malik area with active coal fires, which are indicated by the fire sign. Ravat village is situated on the Yagnob River's bank (top). Outcrops of burned rocks at Kukhi-Malik (left below) and the Big Grotto active gas vent, where iskandarovite was found (right below).

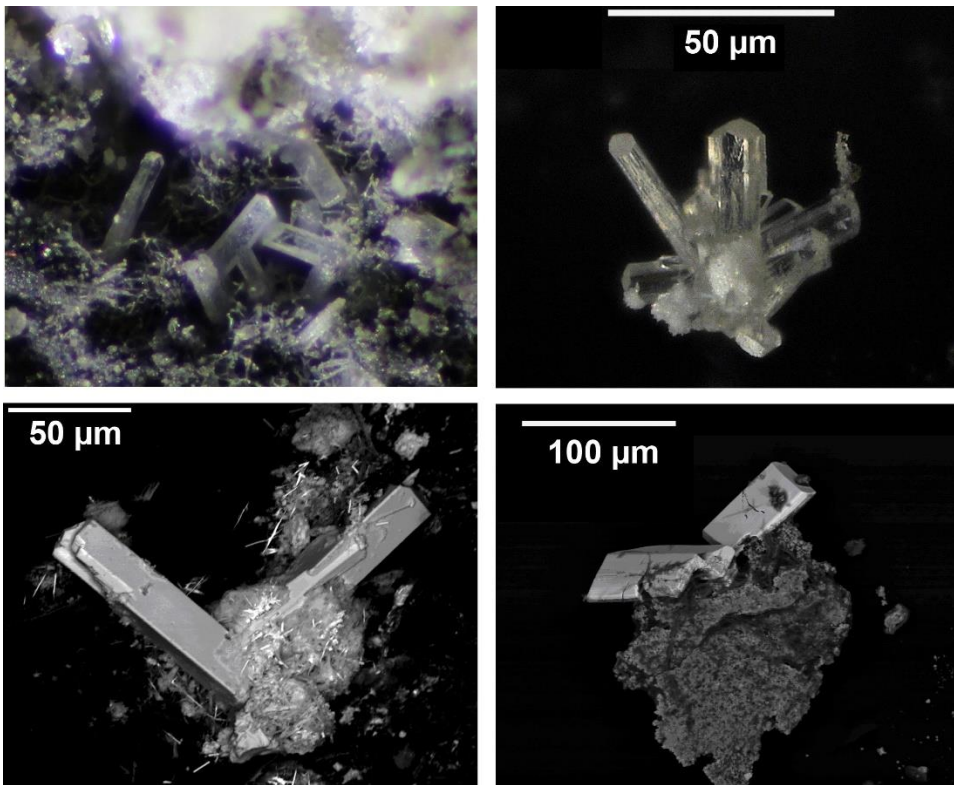


Figure 2. Iskandarovite colorless crystals associated with various sulfates (field of view 2.5 mm) (left above). Cluster of iskandarovite crystals (right above). BSE images of prismatic iskandarovite crystals (below).

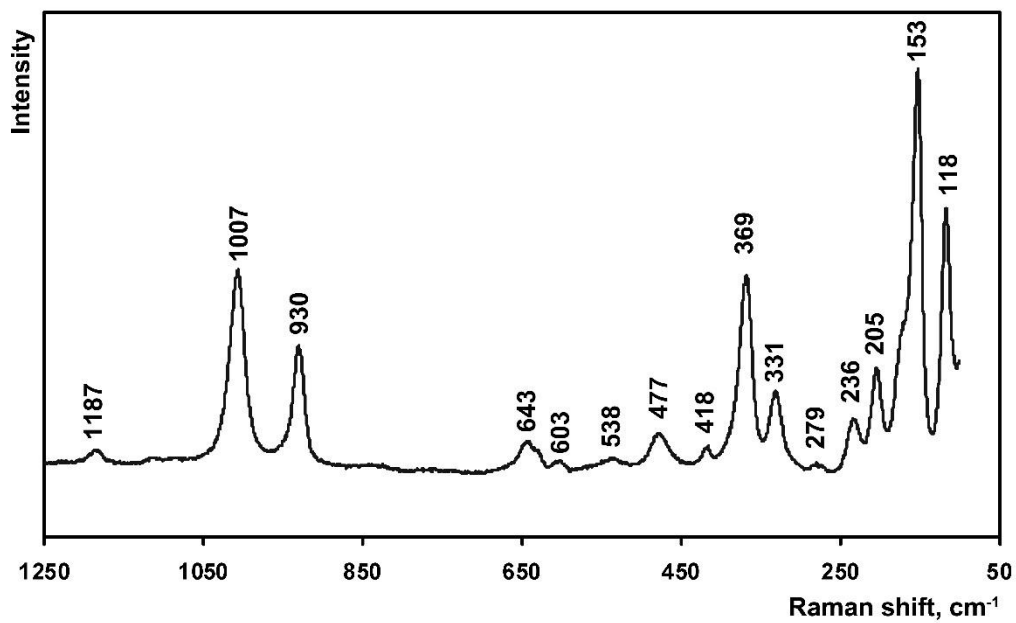


Figure 3. Raman spectra of iskandarovite.

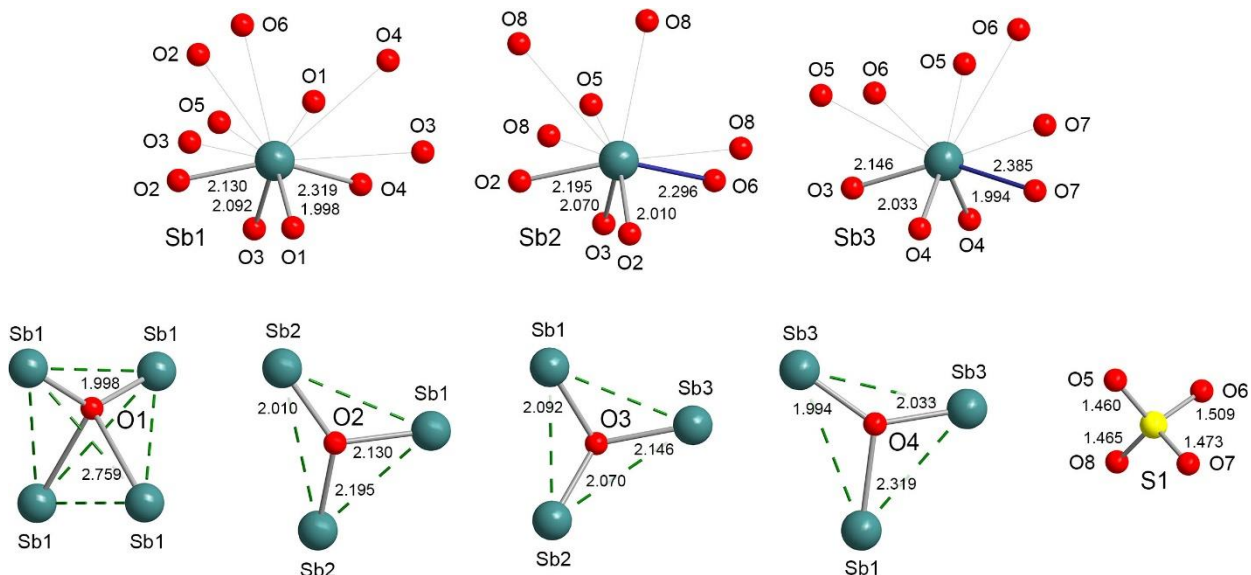


Figure 4. Coordination of cations and anions in the crystal structure of iskanarovite. For Sb atoms (upper row), the strong primary Sb–O bonds $< 2.40 \text{ \AA}$ are indicated by bold lines, and Sb–O secondary bonds $> 2.75 \text{ \AA}$ are shown by thin lines. In the oxocentered OSb₄ and OSb₃ polyhedra, the edges are shown by the green dotted lines.

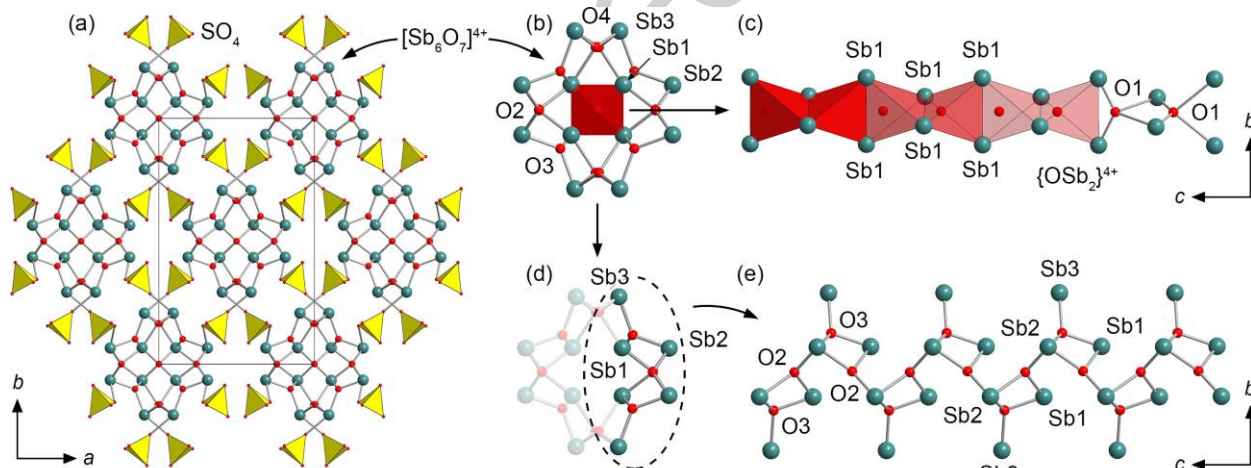


Figure 5. General projection of the crystal structure of iskanarovite along the c axis (a). Enlarged $[\text{O}_7\text{Sb}_6]^{4+}$ rod-like chain (b). The $[\text{O}_7\text{Sb}_6]^{4+}$ rod-like chain is composed of the central $[\text{OSb}_2]^{4+}$ single chain formed by the edge-sharing O1Sb₄ oxocentered tetrahedra (highlighted in red) wrapped by the chains of OSb₃ triangles (d,e).

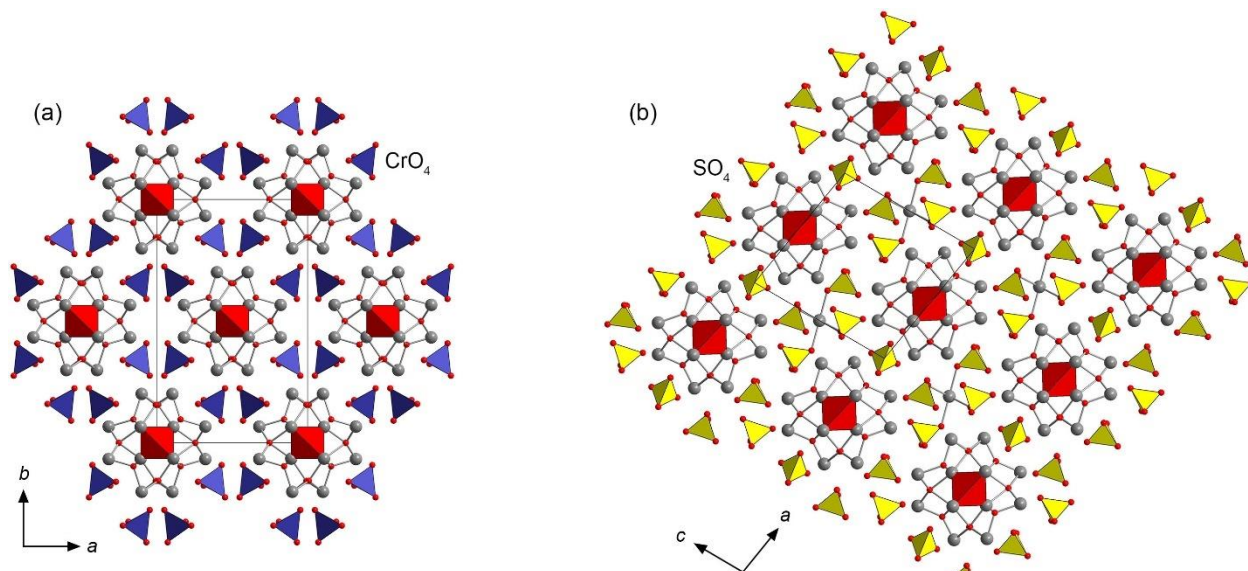


Figure 6. Crystal structure of $\text{Bi}_6\text{O}_7(\text{CrO}_4)_2$ and leguerrite $[\text{Bi}_{12}\text{O}_{14}]\text{Bi}_{0.67}(\text{SO}_4)_5$, structurally related to iskandarovite.

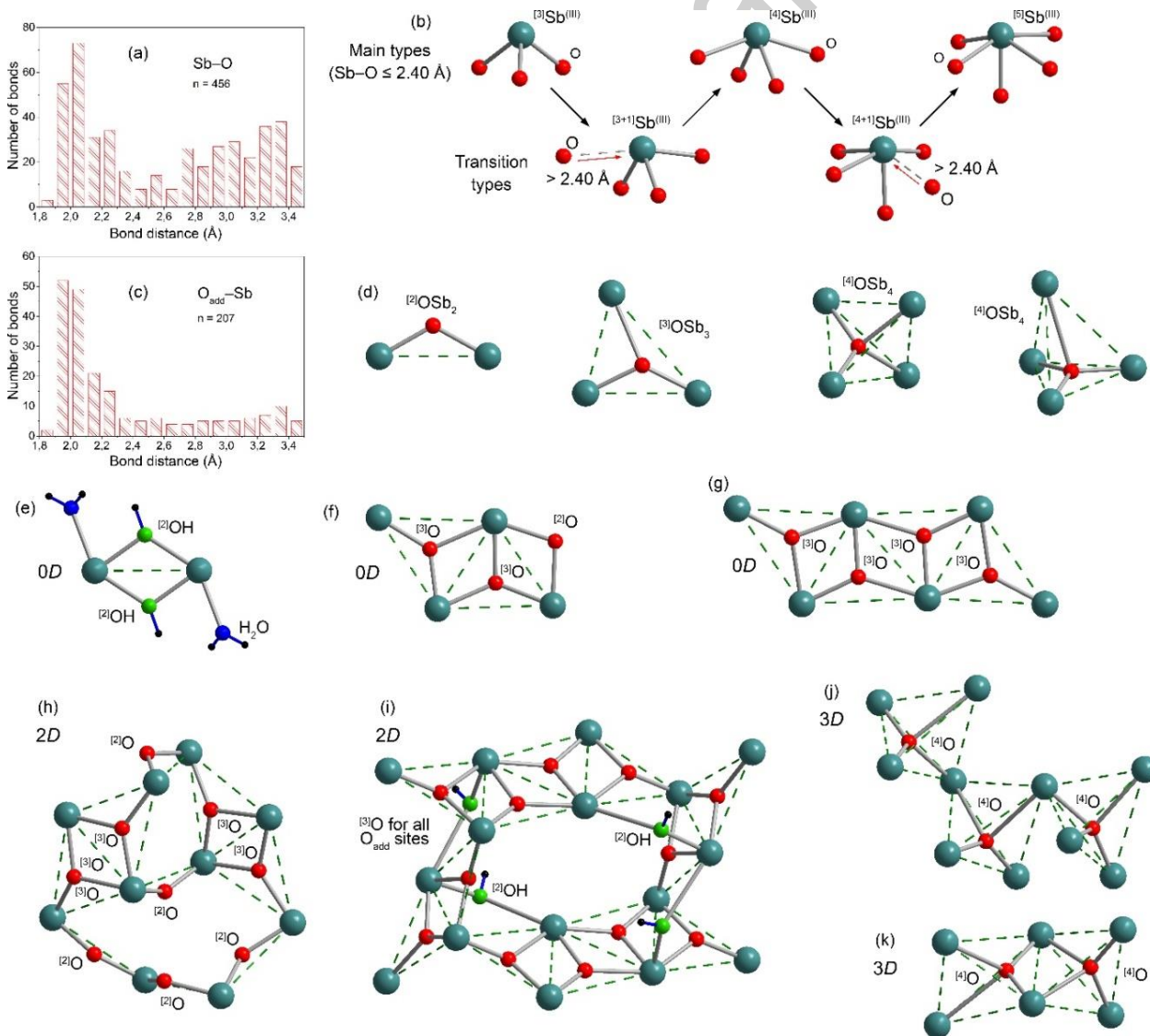


Figure 7. $\{\text{SbO}_n\}$ and $\{\text{OSb}_m\}$ coordination polyhedra in Sb(III) sulfates and oxysulfates. Distribution of bond lengths ≤ 3.5 Å in $\{\text{SbO}_n\}$ polyhedra in the structures of Sb sulfates (a). Main and transition types of $\{\text{SbO}_n\}$ coordination polyhedra in terms of the strong primary bonds (b). Distribution of bond-lengths in $\{\text{OSb}_n\}$ oxocentered polyhedra, $n = 2-4$ (c). $\{\text{OSb}_n\}$ polyhedra in the structures of antimony oxysulfates (d). $[(\text{OH})_2\text{Sb}_2(\text{H}_2\text{O})_2]^{4+}$ units in $\text{Sb}(\text{SO}_4)(\text{OH})(\text{H}_2\text{O})$ (e). $[\text{O}_3\text{Sb}_4]^{6+}$ oxocentered clusters in $(\text{H}_3\text{O})_2\text{Sb}_4\text{O}_3(\text{SO}_4)_4(\text{H}_2\text{O})$ (f) and $[\text{O}_2\text{Sb}_3]^{5+}$ clusters in $\text{NaSb}_3\text{O}_2(\text{SO}_4)_3(\text{H}_2\text{O})$ (g). $[\text{O}_5\text{Sb}_4]^{2+}$ layers in $\text{Sb}_4\text{O}_5(\text{SO}_4)$ (h) and $[\text{O}_2(\text{OH})\text{Sb}_2]^{2+}$ layers in klebelsbergite, $\text{Sb}_4\text{O}_4(\text{SO}_4)(\text{OH})_2$ (i). Framework forming oxocentered building blocks in the crystal structure of coquandite $\text{Sb}_{6.3}\text{O}_{8.3}(\text{SO}_4)(\text{OH})_{0.3}(\text{H}_2\text{O})_{0.7}$ (i,k).

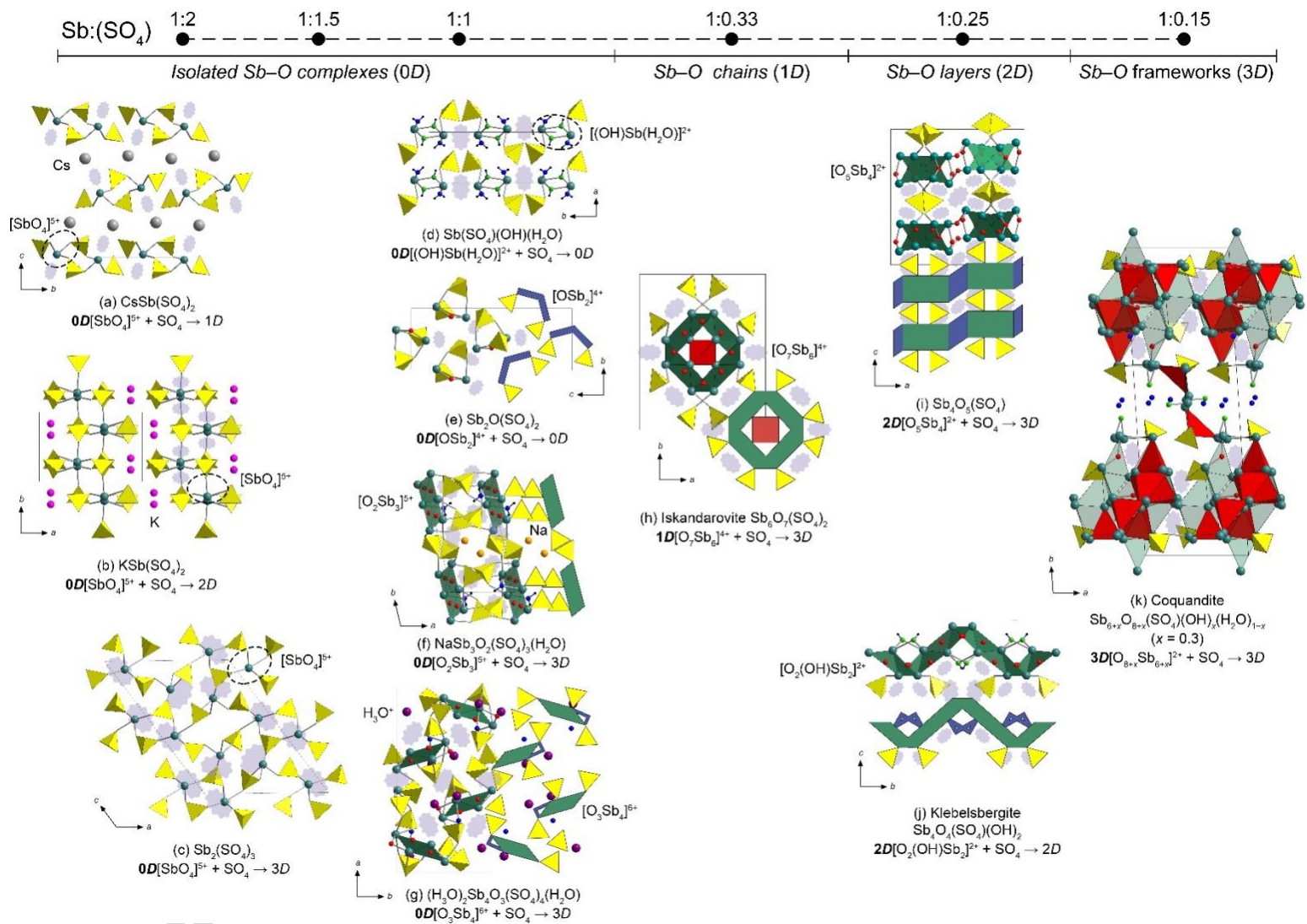


Figure 8. Classification and dimensionality of Sb–O complexes in Sb sulfates and Sb:SO₄ ratio (above). General projections of the crystal structures (SO₄ tetrahedra = yellow; Sb atoms = green balls; O atoms = red balls; H₂O = blue balls; OH = dark-green balls), combined with schematic images (OSb₂ dimers = blue; OSb₃ triangles = green; OSb₄ tetrahedra = red). The probable location of micelles is designated by violet clouds. In the coquandite crystal structure, the central O atoms in the OSb₃ triangles (green) are hidden for clarity.